J Electroceram (2007) 19:9–21
DOI 10.1007/s10832-007-9068-8

Defect structure of oxide ferroelectrics—valence state, site of incorporation, mechanisms of charge compensation and internal bias fields

Invited review for J. Electroceram.

Rüdiger-A. Eichel

Received: 10 October 2006 / Accepted: 9 February 2007 / Published online: 24 April 2007

Abstract The defect structure of aliovalent transition-metal and rare-earth functional centers in ferroelectric perovskite oxides is characterized by means of multifrequency electron paramagnetic resonance spectroscopy, assisted by density-functional theory calculations. The review is mainly focused on lead zirconate titanate ($Pb[Zr_xTi_{1-x}]O_3$, PZT) compounds. However, where available also results on ferroelectric '*lead-free*' compounds are discussed. The results include the formation of charged $(Fe'_{Zr,Ti} - V_O^{\bullet\bullet})^{\bullet}$ defect dipoles, causing internal bias fields, multivalence manganese centers, acceptor-type copper functional centers creating isolated oxygen vacancies that promote ionic conductivity, as well as $Gd_{Pb}^{\bullet}$ donor-type centers. Moreover, the impact of the defect structure on macroscopic material properties is discussed.

Keywords Ferroelectrics · Lead zirconate titanate · PZT · Doping · Defect structure · Valence state · Site of incorporation · Charge compensation · Internal bias fields · Aging · Fatigue · EPR

1 Introduction

Functional ceramics are the *materials-of-choice* in a wide range of applications [1–7], where one of the key advantages is that material properties may be tailored by adding aliovalent transition-metal or rare-earth ions on a percentage level. Because of the low concentration of the so-named functional centers, standard bulk characterization techniques are not well suited for their analysis and electron paramagnetic resonance (EPR) becomes the *method-of-choice* due to its superior sensitivity.

Generally, EPR spectroscopy provides information concerning electronic and structural properties of paramagnetic ions. In particular, important aspects of the defect chemistry and the local defect structure at the site of the functional center may be elucidated, including the valence state and site of incorporation of aliovalent dopant ions. Related to these questions, is the characterization of the prevalent mechanism of charge compensation. Furthermore, EPR may indicate electronic, ionic or polaronic conduction states. Finally, EPR may be used to monitor ferro-to-paraelectric and structural phase transitions, which is beyond the scope of this review.

Principally, the site of incorporation for dopant ions in the perovskite structure may be predicted by considering the corresponding ionic radii, and the *Goldschmidt tolerance factor*

$$t = \frac{r_A + r_O}{\sqrt{2}(r_B + r_O)} \tag{1}$$

that should generally be close to unity [8]. Owing to Eq. 1, dopants will reside on a specific lattice site if a dopant ion's radius is within about 15% of the replaced ion. As a *rule-of-thumb*, the smaller transition-metal ions are incorporated on the perovskite B-site, whereas the larger rare-earth ions will substitute on the A-site. For intermediate ionic radii values, exceptions from this rule were suggested proposing a shared site occupancy. This situation is termed as *amphoteric* and

R.-A. Eichel (✉)
Eduard-Zintl-Institute,
Darmstadt University of Technology,
D-64287 Darmstadt, Germany
e-mail: eichel@chemie.tu-darmstadt.de

a certain kind of dopant ion is incorporated simultaneously on the A- and B-site [9–13]. For trivalent dopants, this scenario comprises a mechanism of *self-compensation*. In particular, it has been speculated that *amphoteric* behavior may maximize the lifetime of components.

Concerning the valence state of the dopant ions, the rare-earth ions usually exhibit their known valency states irrespective of if they are incorporated on the A- or B-site. This is not necessarily the case for the 3*d*-transition metal ions in octahedrally coordinated B-sites. In particular, there exists a stability of certain ions extending over several valencies, as manganese and chromium for instance, allowing for reactions that alter their valency of the type

$$\mathrm{Me}_\mathrm{B}^n \rightleftharpoons \mathrm{Me}_\mathrm{B}^{n+1} + e' \tag{2}$$

$$\mathrm{Me}_\mathrm{B}^n \rightleftharpoons \mathrm{Me}_\mathrm{B}^{n-1} + h^\bullet \tag{3}$$

with e' and $h^\bullet$ being electron and hole states and Me the transition-metal dopant, respectively.

2 Acceptor dopants

Acceptor-dopants generally are of lower valence than the ion they substitute, resulting in a *hard* compound, which in turn is characterized by a comparatively high coercive field required for poling, an increased mechanical quality factor and a smaller electromechanical coupling factor. The predominant charge compensation process for acceptor-type aliovalent dopants is the creation of oxygen vacancies ($V_\mathrm{O}^{\bullet\bullet}$). These are usually the most mobile ionic defects and hence the dominant charge carriers in ceramic oxides. Furthermore, acceptor-doped ceramics with high $V_\mathrm{O}^{\bullet\bullet}$ concentration show increased change of their electrical properties with time, the phenomenon being termed as *aging* [14]. On the other hand, donor-doped ceramics with no significant $V_\mathrm{O}^{\bullet\bullet}$ concentration are more stable in time concerning their electrical properties [1]. The common understanding of the aging phenomenon is that domain-wall motion is increasingly restricted with time [15]. Furthermore, aging is typically accompanied by an increasing shift of the hysteresis loop along the electric field axis [16, 17]. This shift is termed as *internal bias field* and is proposed to occur owing to the relaxation of defect dipoles [18].

2.1 Fe^{3+} and Fe^{3+}-oxygen vacancy associate centers

Compounds modified by Fe^{3+}-doping, typically exhibit low conductivity and an increased dielectric constant. Furthermore, the iron functional center is of considerable interest owing to its photochromic and photorefractive characteristics [19–21]. By using EPR, for Fe^{3+}-modified $PbTiO_3$ an unusually strong tetragonal ferroelectric distortion of the crystalline field typically is observed [22–28]. The corresponding paramagnetic center was assigned to a partially charge-compensated $(Fe'_\mathrm{Ti} - V_\mathrm{O}^{\bullet\bullet})^\bullet$ defect associate [23].

Even though high-frequency EPR (Fig. 1(b,c)) is mandatory in order to elucidate the structure at the Fe^{3+}-site [22], standard X-band EPR (10 GHz) is sufficient to verify the generation of a $(Fe'_\mathrm{Ti} - V_\mathrm{O}^{\bullet\bullet})^\bullet$ defect associate. The characteristic low-field EPR resonance is depicted in Fig. 1(a); the EPR spectrum being dominated by a strong resonance at low field (120 mT). The signal at 300 mT, marked by an asterisk (*), is characteristic for antiferromagnetically coupled Fe_2O_3 species that most probably accumulate at grain boundaries.

In the following, the advent of high microwave frequencies for gaining further micro-structural information is outlined: exploiting sign and size of the axial fine-structure parameter B_2^0, it was shown on the basis of semi-empirical Newman superposition model calculations that the Fe^{3+} functional center in lead titanate forms a charged $(Fe'_\mathrm{Ti} - V_\mathrm{O}^{\bullet\bullet})^\bullet$ defect associate with an oxygen vacancy in the first coordination sphere [23]. Furthermore, it could be deduced that the iron ion is substituted at the B-site of the perovskite ABO_3 lattice. This assignment is supported by the similarity of ionic radii between Ti^{4+} at 68 pm and Fe^{3+} at 64 pm as compared to Pb^{2+} with a radius of 124 pm. Moreover, the generation of an $(Fe'_\mathrm{Ti} - V_\mathrm{O}^{\bullet\bullet})^\bullet$ defect dipole is in accordance with first-principle calculations that more generally predict the binding of oxygen vacancies to acceptor-type impurities [30]. Experimental findings indicate, however, that for other acceptor centers in similar compounds, like copper-modified PZT [31] and chromium-doped $PbTiO_3$ [32], no such association seems to be present.

Because the observed Fe^{3+}:$PbTiO_3$ EPR spectra [22] can exclusively be interpreted in terms of $(Fe'_\mathrm{Ti} - V_\mathrm{O}^{\bullet\bullet})^\bullet$ associates, it was concluded that no free Fe'_Ti signals, i.e. iron ions without associated $V_\mathrm{O}^{\bullet\bullet}$ are present. Considering the condition for overall charge compensation, there is thus a charge mismatch because the Fe^{3+} ion substituting for the Ti^{4+} ion is singly negative charged (Fe'_Ti), whereas the associated oxygen vacancy is doubly positive charged ($V_\mathrm{O}^{\bullet\bullet}$) with respect to the neutral lattice. Hence, additional mechanisms for charge compensation have to be discussed. Candidates for charge compensation are either free electrons (e') trapped in the lattice, lead vacancies (V''_Pb), and the formation of positively charged cations, such as $Pb^{2+} \rightarrow$

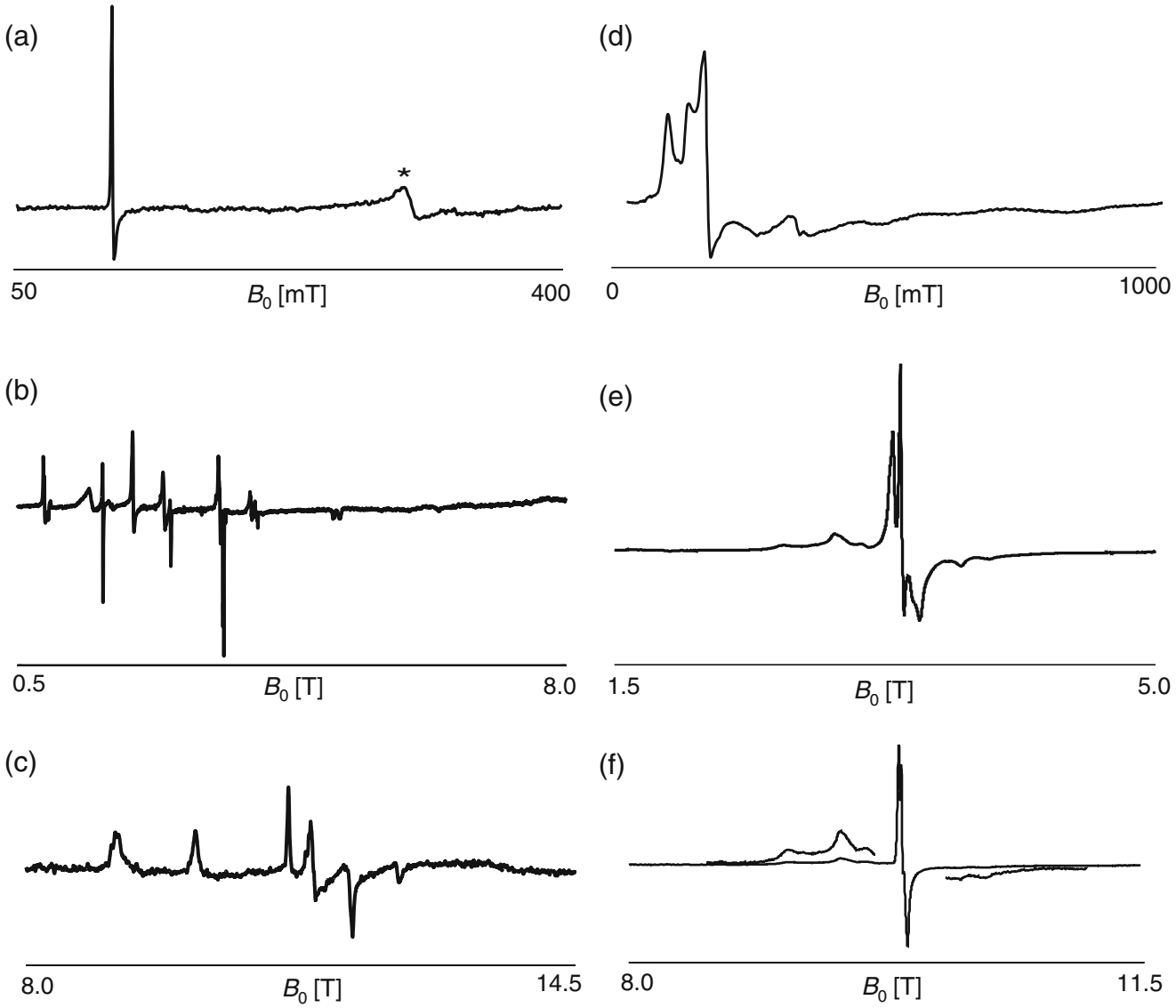

Fig. 1 Multifrequency EPR spectra of 0.5 mol %-doped Fe^{3+}:$PbTiO_3$ (**a**–**c**) and $PbZrO_3$ (**d**–**f**). (**a**, **d**) X-band (9.4 GHz). (**b**, **e**) W-band (95 GHz). (**d**) 319 GHz. (**f**) 280 GHz

Pb^{+}, $Ti^{4+} \rightarrow Ti^{3+}$, or $Fe^{3+} \rightarrow Fe^{2+}$. However, there is no evidence for color centers in the *DFT* calculations [23] and the variable valency ions Pb^{+}, Ti^{3+} are paramagnetic with g-values at about $g \approx 2.0$ to 1.9, which were also not observed in the EPR spectra and thus can be excluded [22]. Consequently, intrinsic double negatively charged lead vacancies V''_{Pb} have been suggested as additional charge compensation. The overall electroneutrality condition for iron-modified lead-containing components ($PbTiO_3$, $PbZrO_3$, PZT) thus is proposed to be given by means of the following incorporation reaction

$$PbO + Fe_2O_3 \longrightarrow Pb^{\times}_{Pb} + 4O^{\times}_{O} + 2\left(Fe'_{Zr,Ti} - V^{\bullet\bullet}_{O}\right)^{\bullet} + V''_{Pb} \quad (4)$$

This model is supported by the inherent loss of PbO during high-temperature processing, for which reason a natural intrinsic $(V^{\bullet\bullet}_{O} - V''_{Pb})^{\times}$ di-vacancy pair was proposed [33], its existence, however, being currently controversially discussed on the basis of *DFT* calculations [34, 35].

It has been much speculated about the orientation of the $(Fe'_{Ti} - V^{\bullet\bullet}_{O})^{\bullet}$ defect dipole with respect to the orientation of the spontaneous polarization [29]. From the symmetry of the corresponding FS interaction tensor it may be inferred that the $(Fe'_{Ti} - V^{\bullet\bullet}_{O})^{\bullet}$ center conserves the four-fold site symmetry at the lattice B-site [22]. Consequently, the $(Fe'_{Ti} - V^{\bullet\bullet}_{O})^{\bullet}$ defect dipole has to be persistently oriented along the crystallographic c-axis. *DFT* calculations predict that the arrangement in which the $(Fe'_{Ti} - V^{\bullet\bullet}_{O})^{\bullet}$ defect dipole is being oriented

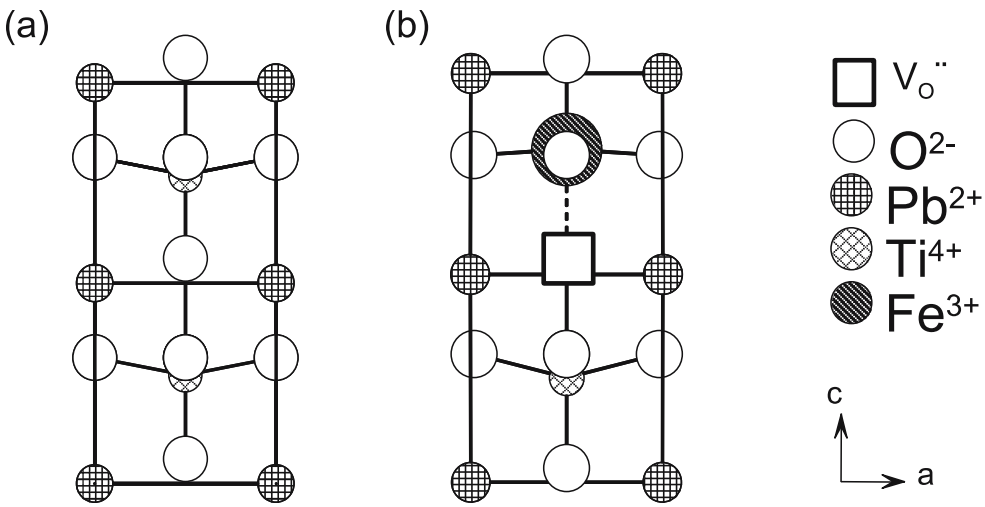

Fig. 2 Micro-structural configuration for the lead titanate unit cell. (**a**) Undoped $PbTiO_3$ compound. (**b**) 0.5 mol %-doped Fe^{3+}:$PbTiO_3$. Data reproduced from [23]

antiparallel with respect to the overall spontaneous polarization is the lowest in energy of formation, as illustrated in Fig. 2 [23]. This single-site situation is supported by the EPR results, which find evidence for only a single $(Fe'_{Ti} - V_O^{\bullet\bullet})^{\bullet}$ center [22]. Analogously, for pure $PbTiO_3$ it has been predicted on the basis of *DFT* calculations that oxygen vacancies are preferentially created at the apical oxygen position, rather than at the equatorial positions [36]. The experimental results hence support earlier suggestions made for $BaTiO_3$ compounds, after which defect dipoles may align along the direction of spontaneous polarization [37].

Concerning the structural arrangement in the vicinity of the $(Fe'_{Ti} - V_O^{\bullet\bullet})^{\bullet}$ center, the Fe'_{Ti} ion relaxes back into the plane of equatorial oxygens, as represented in Fig. 2 [23]. As a consequence, the bond distance to the remaining apical oxygen ion is considerably reduced, for which reason the originally van-der-Waals type bonding is transformed into a rather covalent type of bonding, coinciding with a reduced energy of formation [23]. A similar scenario has been reported for the $(Fe'_{Ti} - V_O^{\bullet\bullet})^{\bullet}$ center in $BaTiO_3$ [11].

The ABO_3 perovskite structure containing an $V_O^{\bullet\bullet}$ and an acceptor impurity D'_B has also theoretically been considered [38]. The probability of finding an oxygen vacancy in the nearest neighbor position of the D'_B acceptor center is predicted to be highest along the crystallographic *c*-axis. In this so-called *symmetry-conforming point defect* configuration, the spontaneous polarization associated with the polar tetragonal crystal symmetry, and the defect polarization, associated with the non-centric distribution of charged point defects, are oriented in antiparallel with respect to each other. As consequence, the decrease in reversible domain switching in aged ferroelectrics was proposed being due to such symmetry-conforming point defects [38]. Whereas the defects were shown to be unstable in the non-aged state they were transformed to a stable state after aging; the defect symmetry following the crystal symmetry. A similar model has already been proposed on the basis of a gradual alignment of $(Fe'_{Ti} - V_O^{\bullet\bullet})^{\bullet}$ defect dipoles in $BaTiO_3$ and PZT [39, 40].

More generally, macroscopic dielectric and ferroelectric properties strongly depend on the domain configuration, which in turn is considerably impacted by the microstructure made up by different defects [18, 41–43]. In particular, aging is discussed in terms of the clamping of 90°-domain walls by oriented dipolar defects in adjacent domains. It has been shown, that charged defect agglomerates may influence the poling properties by providing pinning centers for domain walls [44]. Furthermore, the possibility that dipolar defect complexes can also pin the polarization of the surrounding crystal has been demonstrated by *DFT* calculations [30]. In particular, oxygen-vacancy related defect dipoles have been shown to be involved in voltage offsets leading to imprint failure [45] and are suggested to play a crucial role in electrical fatigue [30, 46, 47]. With respect to the ionic mobility of free oxygen vacancies, the iron - oxygen vacancy defect dipole complex will be rather immobile in the ceramic. Hence, charge transport will be considerably hindered. On the other hand, the reorientation of the defect dipole may give raise to ferroelectric aging.

For Fe^{3+}-modified lead zirconate EPR has detected a considerably reduced FS splitting as compared to Fe^{3+}-doped $PbTiO_3$ [48]. The corresponding EPR spectra are depicted in Fig. 1(d–f). Contrary to the *single-site* $PbTiO_3$ case, for which a single orientation of the $(Fe'_{Ti} - V_O^{\bullet\bullet})^{\bullet}$ dipole was observed, the obtained result points to a *multiple-site* situation in $PbZrO_3$, generated by different possible orientations of the $(Fe'_{Zr} - V_O^{\bullet\bullet})^{\bullet}$

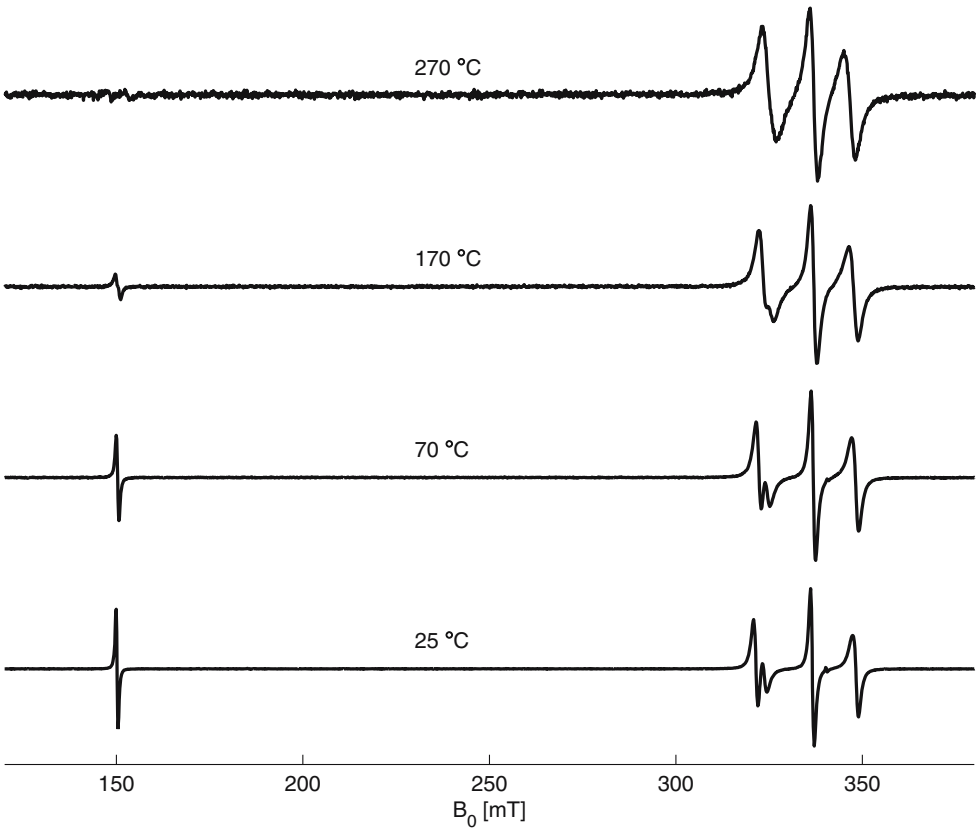

Fig. 3 X-band EPR spectra showing the temperature-dependent equilibrium between the $(Fe'_{Ti} - V_O^{\bullet\bullet})^{\bullet}$ defect associate centered at 150 mT and 'free' Fe'_{Ti} centers at 337 mT in $SrTiO_3$. Data reproduced from [50]

dipole owing to the fact that the oxygen vacancy may take several or all of the nearest-neighbor oxygen sites in $PbZrO_3$. Consequently, the $(Fe'_{Zr} - V_O^{\bullet\bullet})^{\bullet}$ dipole is expected being easier to reorient in lead zirconate as compared to lead titanate. Thus, the above mentioned effects of domain-wall clamping most probably are reduced for iron-modified lead zirconate as compared to lead titanate.

The kinetic behavior of a situation in which an oxygen vacancy is a mobile particle in the oxygen octahedron enclosing an acceptor ion has been described in a *relaxation model* for the $(Ni''_{Ti} - V_O^{\bullet\bullet})^{\times}$ center in $BaTiO_3$ [29]. Within this model, the relaxation time of ferroelectric ceramics is determined by the thermally activated diffusive jumping of the oxygen vacancies. Analogously to the symmetry-concorming point defect model, an alignment of the defect dipoles leads to an increased internal bias that may lead to a clamping of domain walls [49].

Alternatively, in iron-doped $SrTiO_3$, a temperature-dependent equilibrium between 'free' Fe'_{Ti} centers and $(Fe'_{Ti} - V_O^{\bullet\bullet})^{\bullet}$ defect associates can be present [50], according to

$$Fe'_{Ti} + V_O^{\bullet\bullet} \leftrightharpoons (Fe'_{Ti} - V_O^{\bullet\bullet})^{\bullet} \quad (5)$$

As the approximate electroneutrality condition is in this case

$$2[V_O^{\bullet\bullet}] \approx [Fe'_{Ti}] \quad (6)$$

at most half of the Fe'_{Ti}, but all of the $V_O^{\bullet\bullet}$ can be bound in $(Fe'_{Ti} - V_O^{\bullet\bullet})^{\bullet}$ defect associates. The corresponding temperature-dependent EPR spectra are depicted in Fig. 3. Obviously, the number of the $(Fe'_{Ti} - V_O^{\bullet\bullet})^{\bullet}$ defect associates that occur at 150 mT in the EPR spectra decreases with increasing temperature, relative to the intensity of the 'free' Fe'_{Ti} centers centered at 335 mT. Upon reduction of temperature, the association of Fe'_{Ti} with an $V_O^{\bullet\bullet}$ is increasingly generated. For the dissociation of an existing $(Fe'_{Ti} - V_O^{\bullet\bullet})^{\bullet}$ dipole, only one elementary jump of the oxygen vacancy from the first to the second coordination sphere is necessary, whereas for the association of a new associate typically more jumps are required. Jump rates from $7 \cdot 10^6\ s^{-1}$ at 500 K down to $12\ s^{-1}$ at 300 K have been estimated for $SrTiO_3$ [50]. Hence, an equilibrium is still possible at room temperature or slightly below.

Even though, the Fe^{3+} oxidation state is generally observed in perovskite oxides, under strong reducing conditions also the Fe''_{Ti} and Fe'''_{Ti} centers, and the corresponding $(Fe''_{Ti} - V_O^{\bullet\bullet})^{\times}$ and $(Fe'''_{Ti} - V_O^{\bullet\bullet})'$ associates

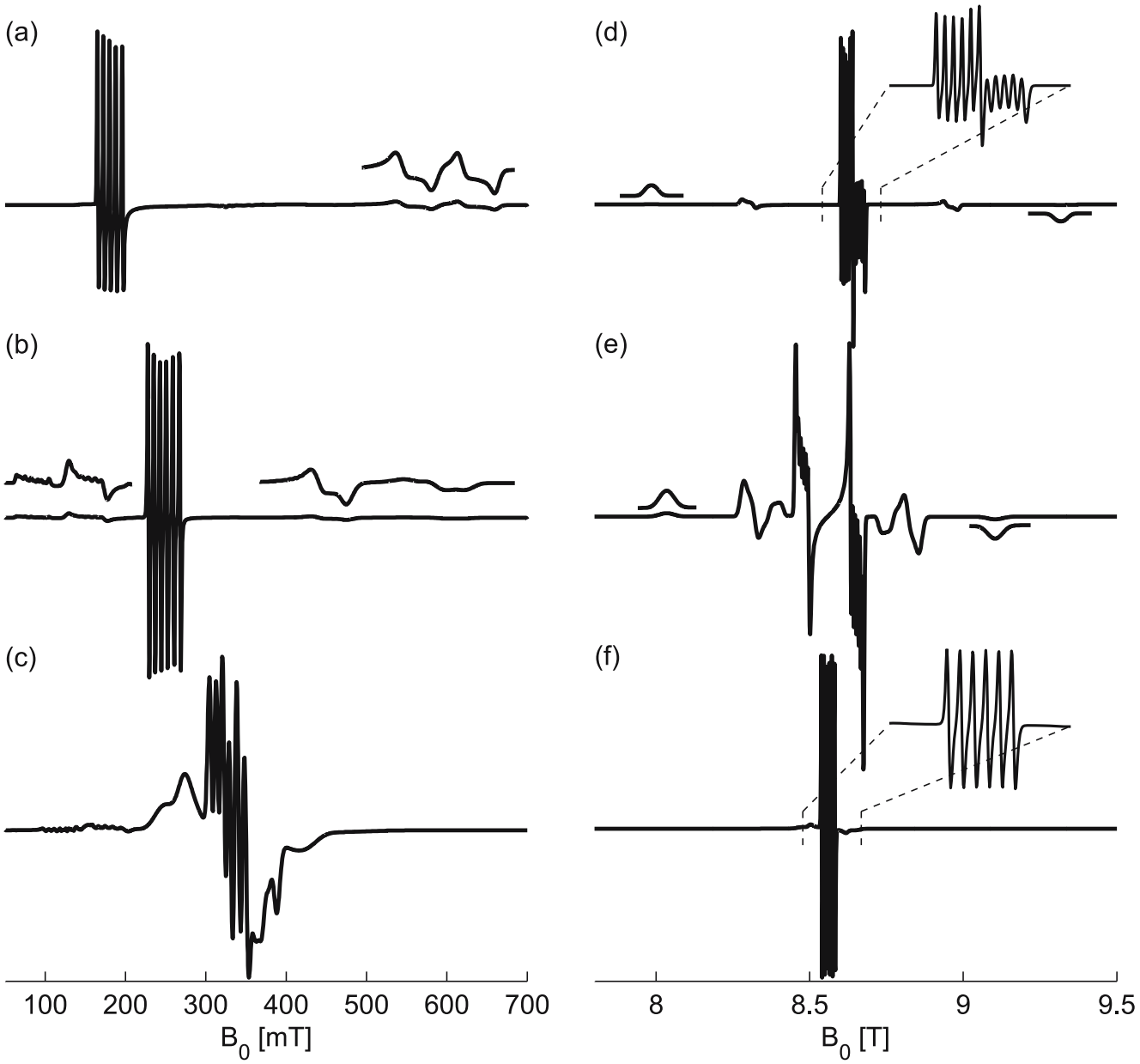

Fig. 4 Multivalency manganese centers in $PbTiO_3$. Numerical spectrum simulation at X-band (**a**–**c**) and at 240 GHz (**d**–**f**). (**a**, **d**) $Mn^{\times}_{Ti}$:$PbTiO_3$. (**b**, **e**) Mn'_{Ti}:$PbTiO_3$. (**c**, **f**) Mn''_{Ti}:$PbTiO_3$

have been identified in $SrTiO_3$ [51]. Moreover, the $(Fe'_{Ti} - V^{\bullet\bullet}_O)^{\bullet}$ center may be reloaded upon exposure to sub-band gap light, as also valency altered $(Fe'''_{Ti} - V^{\bullet\bullet}_O)'$ [51] and $(Fe''_{Ti} - V^{\bullet\bullet}_O)^{\times}$ [52] centers in $SrTiO_3$ were observed. On the other hand, an $(Fe^{\times}_{Ti} - V^{\bullet\bullet}_O)^{\bullet\bullet}$ dipole was observed in oxidized $SrTiO_3$ and Mg''_{Ti}- or Al'_{Ti}-doped single crystals [19]. Analogous defect associates have been observed also in similar compounds; in $BaTiO_3$ an $(Fe'_{Ti} - V^{\bullet\bullet}_O)^{\bullet}$ center [53] and in $KTaO_3$ an $(Fe'_{Ta} - V^{\bullet\bullet}_O)^{\bullet}$ center have been observed [9, 54].

Although, recent results exclusively report the incorporation of Fe^{3+} on the perovskite B-site, also an *amphoteric* situation with ordinary $Fe^{\bullet\bullet}_K$ centers and additional Fe''_{Ta} centers has been proposed for $KTaO_3$ single crystals [9].

2.2 Multivalence Mn^{2+}, Mn^{3+} and Mn^{4+} centers

Manganese functional centers possess of the particular property that they may occur in several oxidation states. The most important information provided by EPR when studying manganese-modified components, is the ability of determining the manganese

oxidation state and its site of incorporation. Generally, manganese-doping of $PbTiO_3$ renders compounds with high mechanical strength, low dielectric losses and low dielectric constant, which is essential for instance for piezoelectric resonator applications. Moreover, increasing manganese-doping decreases the electric conductivity in lead titanate [55], being important for high-temperature applications. Manganese is incorporated on the titanium site in $BaTiO_3$ and $PbTiO_3$, exhibiting oxidation states of $Mn_{Ti}^{\times}$, $Mn_{Ti}^{\prime}$ and $Mn_{Ti}^{\prime\prime}$. After oxidizing pretreatment at 800 °C in air, the $Mn_{Ti}^{\times}$ state dominates [56]. Reducing treatment in nitrogen atmosphere leads rather to the presence of $Mn_{Ti}^{\prime}$ and $Mn_{Ti}^{\prime\prime}$ centers [57, 58]. Alternatively, co-doping with donor-type $La_{Pb}^{\bullet}$ leads also to the formation of aliovalent $Mn_{Ti}^{\prime\prime}$ centers [58]. As a function of partial pressures of O_2 and PbO, simultaneously $Mn_{Ti}^{\prime\prime}$, and $Mn_{Ti}^{\times}$ charge states have been identified, where high partial pressures of O_2 and PbO promote the existence of $Mn_{Ti}^{\times}$ in lead titanate [59]. A systematic study of the influence of preparation conditions on the valence state of manganese has been reported in [60].

Concerning the site of incorporation, it was speculated about a simultaneous incorporation of the manganese ions onto A- and B-sites for charge compensation, preferring $Mn_{Pb}^{\times}$ on the A-site [59], this suggestion however still being under debate. Such an *amphoteric* situation with ordinary $Mn_{Ti}^{\prime\prime}$ centers and additional $Mn_{Sr}^{\times}$ centers has also been proposed for $SrTiO_3$ [10, 11].

EPR at X-band may be applied in order to identify the different charge states by their *fingerprint*-type EPR pattern, as shown in Fig. 4(a–c) for model-type numerically simulated manganese EPR spectra. A first assignment to either of the possible manganese oxidation states may be made on basis of their ^{55}Mn-hyperfine splitting and their electronic g-value (cf. Table 1). In particular, the EPR spectra are dominated by the ^{55}Mn-sextet hyperfine pattern. As the FS interaction is larger than the electron Zeeman interaction for the Mn^{4+} and Mn^{3+} states, signals are observed at low magnetic fields corresponding to '*effective*' g-values of $g' = 5.9$ and 3.8 (Fig. 4(a, b)), respectively [61]. Only in case of the Mn^{2+} state, the high-field regime is established and the spectrum is centered about $g = 2.001$ (Fig. 4(c)).

For a more thorough investigation of the micro structure, the fine structure interaction parameter B_2^0 has to be accurately determined. The determination of $|B_2^0|$ at X-band frequencies is only possible via the position of the high-field transitions at 400–700 mT, which are a function of B_2^0 in second order. A more exact determination of the value for B_2^0 may only be obtained by high-frequency EPR investigations via first-order shifts, as depicted in Fig. 4(d–f) for spectra simulated for a Larmor frequency of 240 GHz. Additionally, the sign of B_2^0 may be determined at low temperatures. The accurately determined size and sign of the FS interaction parameters then allows for a further assignment of the prevailing manganese oxidation state (cf. Table 1). Furthermore the association to charge-compensating oxygen vacancies may be determined by using semi-empirical superposition calculations in analogy to the case for the $(Fe_{Ti}^{\prime} - V_O^{\bullet\bullet})^{\bullet}$ center. Such $(Mn_{Ti}^{\prime\prime} - V_O^{\bullet\bullet})^{\bullet}$ defect dipoles have already been observed in $SrTiO_3$ [50].

The multi-valency behavior of manganese may be discussed in terms of providing trapping centers for electrons according to reloading reactions of the form

$$Mn_{Ti}^{\times} + e' \leftrightharpoons Mn_{Ti}^{\prime} \quad (7)$$

$$Mn_{Ti}^{\prime} + e' \leftrightharpoons Mn_{Ti}^{\prime\prime} \quad (8)$$

The produced electrons are preferentially trapped on the manganese sites because the $Mn_{Ti}^{\times}$ and $Mn_{Ti}^{\prime}$ ions are more reducible than the regular $Ti_{Ti}^{\times}$ ions [63].

By monitoring the manganese functional center in $BaTiO_3$, EPR was used to account for explaining the degradation of resistivity by developing a model in which the macroscopically observed phenomena were described by means of an injection of oxygen vacancies from the anode, accompanied by a reduction of the manganese valence, forming $Mn_{Ti}^{\prime\prime}$ centers by the degradation process [64].

2.3 Cu^{2+} center

The Cu^{2+} center is often used as additive during sintering in order to obtain dense ceramics. Consequently, it is important to enlighten in which way Cu^{2+}-dopants impact the defect chemistry. In copper-doped $PbTiO_3$,

Table 1 *Fingerprint*-type spin-Hamilton parameters for the indentification of different manganese oxidation states.

oxidation state	g-value	$\lvert a_{iso}\rvert$ [MHz]	$\lvert B_2^0\rvert$ [GHz]
Mn^{4+}	1.994 ± 0.002	220 ± 10	9.1 ± 0.2
Mn^{3+}	1.997 ± 0.001	–	–
Mn^{2+}	2.001 ± 0.001	240 ± 20	0.6 ± 0.1

a single copper centre of axial symmetry has been found, the observed g-values being consistent with a coordination at the Ti site [24, 65]. In polycrystalline Cu:[Pb_yLa_{1-y}]TiO_3, a single axial centre with $g_\parallel > g_\perp > g_e$ was found in accordance with the tetragonal crystal structure [66]. For the solid solution system Cu:Pb[Zr_xTi_{1-x}]O_3 with various compositions x ranging from 0 to 0.9, the Cu^{2+} ion was proposed to be situated in two different environments, one with $g_\parallel > g_\perp > g_e$ and the other with $g_\perp > g_\parallel > g_e$ [67]. The sign change of the g-matrix anisotropy was rationalized by assuming the formation of a tetragonally compressed octahedron, arguing that the addition of Zr to the lattice causes increased distortion at the B-site, thus being responsible for this deformation. However, a recent high-field EPR investigation disproved this assignment [70], and the second observed center is rather due to a center of rhombohedral symmetry. EPR was also employed in copper-doped electro-optic [$Pb_{0.92}La_{0.08}$][$Zr_{0.65}Ti_{0.35}$]O_3 (PLZT 8/65/35) ceramics [68], in which the observed EPR spectra were simulated by a superposition of axial and isotropic Cu^{2+} spectra of unknown origin. In Cu^{2+}:$BaTiO_3$ ceramics, also two superposed copper centers were observed [69]. Depending on doping level and sintering temperature, the EPR data exhibited two different Cu''_{Ti} spectra with $g_\parallel > g_\perp > g_e$ each, attributed to tetragonally distorted CuO_6 octahedra in tetragonal and rhombohedral crystal surroundings, respectively.

In Fig. 5, the X-band EPR spectra of Cu^{2+}-modified PZT 54/46 as compared to the corresponding spectra for the pure members Cu^{2+}:$PbTiO_3$ and Cu^{2+}:$PbZrO_3$ are shown. In particular, the g_{zz}-region is well resolved. However, the values strongly vary when changing from lead titanate ($g_{zz} = 2.332 \pm 0.001$, $A_{zz}^{Cu} = 395.0 \pm 0.5$ MHz) to lead zirconate ($g_{zz} = 2.451 \pm 0.001$, $A_{zz}^{Cu} = 210.5 \pm 0.5$ MHz) [24, 70]. The observed variations in g-values may be traced back to changes in covalency of the $Cu^{2+}-O^{2-}$ bonding, increasing with the Ti-content in the neighborhood of the Cu^{2+} functional center [70].

Concerning the site of incorporation for the Cu^{2+} ion, the observed g-values with $g_{zz} > g_{yy}, g_{xx}$, are characteristic for Cu^{2+} coordinated by six ligands that form an elongated octahedron [71]. This can be understood in terms of a five-fold orbital degeneracy of the $3d^9$ ion that is lifted in the presence of an octahedral crystal field yielding a triplet (t_{2g}) and a doublet (e_g), with the latter lying lowest. The lattice distortion splits the e_g levels further, resulting in an orbital-singlet $d_{x^2-y^2}$ ground state. Consequently, it can be inferred that the Cu^{2+} ion substitutes at the $[Zr,Ti]^{4+}$-site, acting as an electron acceptor. The similarity of effective ionic radii between Ti^{4+} at 68 pm, Zr^{4+} at 81 pm and Cu^{2+} at 72 pm as compared to Pb^{2+} with a radius of 124 pm supports this assignment.

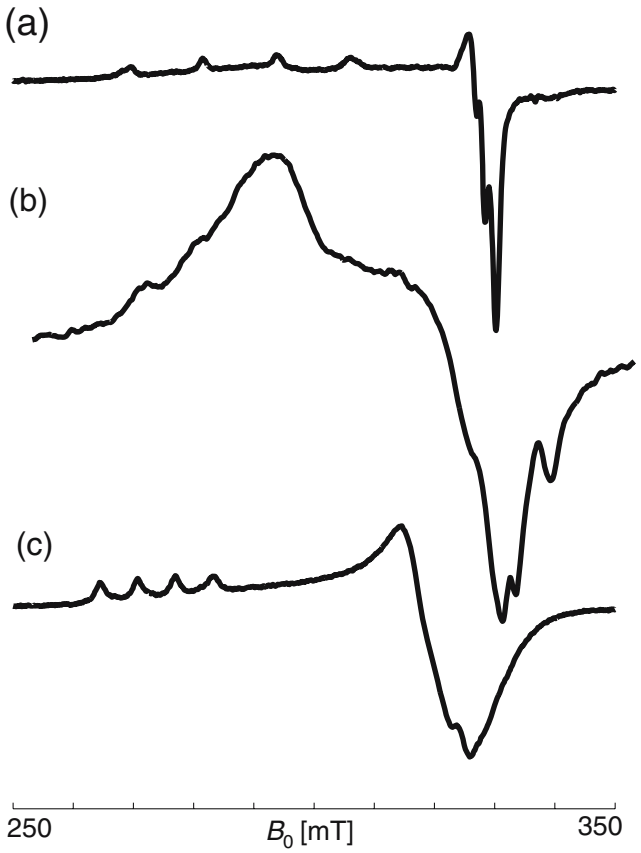

Fig. 5 X-band EPR spectra of 0.25 mol %-doped Cu:Pb[Zr_xTi_{1-x}]O_3. (**a**) Cu^{2+}:$PbTiO_3$. (**b**) and Cu^{2+}:Pb[$Zr_{0.54}Ti_{0.46}$]O_3. (**c**) Cu:$PbZrO_3$. Data reproduced from [24]

By the use of hyperfine sublevel correlation (HYSCORE) spectroscopy, the hyperfine interaction to neighboring ^{207}Pb ions to the copper(II) center may be probed. In Fig. 6, the corresponding HYSCORE spectrum is shown [31]. In particular, it is observed that the isotropic part of the hyperfine splitting (8.8 ± 0.2 MHz) is considerably larger than the anisotropic part (1.5 ± 0.2 MHz). Moreover, the ^{207}Pb hyperfine features and linewidths are identical for all observer field settings. Consequently, there is no orientation dependence with respect to the local coordinate system of the $Cu''_{[Zr,Ti]}$ functional center [31]. Because an oxygen vacancy directly coordinated to the $Cu''_{[Zr,Ti]}$ center would define a local g-tensor orientation, any statistical orientational distribution would be prevented. Thus, the ^{207}Pb-hyperfine data gives no indication of an oxygen vacancy in the vicinity of the $Cu''_{[Zr,Ti]}$ center and charge compensation has to take place in distant coordination spheres according to the following reaction of incorporation

$$PbO + CuO \longrightarrow Pb_{Pb}^{\times} + Cu''_{Ti} + 2O_O^{\times} + V_O^{\bullet\bullet} \qquad (9)$$

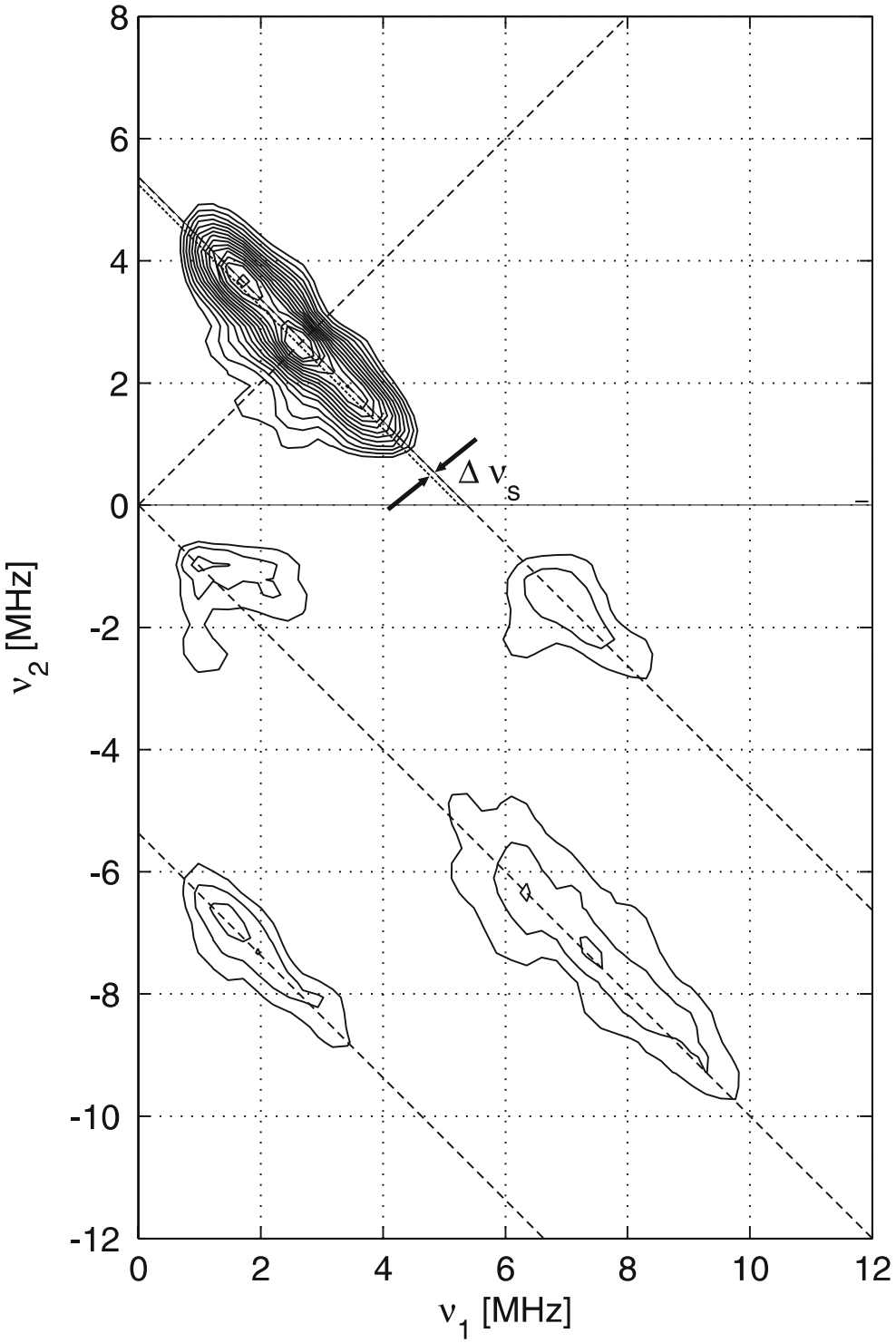

Fig. 6 X-band ^{207}Pb-HYSCORE spectrum recorded at an observer position of 300 mT. In the (+, +) quadrant, the dashed lines show the frequency diagonal axis $\nu_1 = \nu_2$; the antidiagonal (*dotted line*) crosses the diagonal at (ν_b, ν_{Pb}). The maximum vertical shift $\Delta\nu_s$ of the cross-peak ridges from the antidiagonal is illustrated by a *solid line*. In the (−, +) quadrant, two parallels to the diagonal axis $-\nu_1 = \nu_2$ are indicated (*dashed*), with an interdistance of $2\nu_{Pb}$. Data reproduced from [31]

Hence, for Cu^{2+}-modified PZT compounds, the following scenario concerning the defect structure emerges: oxygen vacancies may be considered as isolated point defects that may migrate through the lattice [72]. Whereas the cation sublattice typically is *frozen-in* for perovskites, oxygen vacancies may migrate under electrical potential gradients comparatively easy. This is owing to the ABO_3 perovskite structure, in which each oxygen vacancy has oxygen second-nearest neighbors with which the position may be exchanged. This is in contrast to the situation for Fe^{3+} modifications in PZT and also contradicts first-principle calculations that always predict the binding of oxygen vacancies to acceptor-type impurities, irrespective to their chemical

nature [30]. Experimental findings indicate however, that also for other acceptor centers in similar compounds, like chromium-doped $PbTiO_3$ [32], as well no such defect association is present. Correspondingly, this difference in the micro-structural configuration of different acceptor-type functional centers may provide a basis to enlighten the different effects Fe^{3+} and Cu^{2+} modifications have on the macroscopic ferroelectric properties of PZT compounds. In particular, considerably reduced aging rates are expected for copper-modified compounds, as compared to iron-doped materials because the aging rate is proportional to the internal bias field [77]. This situation is supported by the observation that in $BaTiO_3$ double charged acceptors (Ni''_{Ti}) cause less nonlinearities in the dielectric response - which is an aspect of aging - than single charged acceptor ions (Al'_{Ti}, Cr'_{Ti}) [49]. On a microscopic level, this phenomenon may be understood by considering on the one hand rather isolated defects ($Cu''_{[Zr,Ti]}$, $V_O^{\bullet\bullet}$) in case of copper-doping and on the other hand a charged defect dipole $(Fe'_{[Zr,Ti]} - V_O^{\bullet\bullet})^{\bullet}$ in case of an iron modification, which increases the dielectric response through the existence of the internal bias field of the dipole. Furthermore, the role of oxygen vacancies has attracted special attention with respect to ferroelectric fatigue because the $V_O^{\bullet\bullet}$ are the predominant and most mobile defects in perovskite oxides. Therefore, it has been suggested that the migration of $V_O^{\bullet\bullet}$ plays an important role in the fatigue mechanism [73–76]. By considering the two different defect stuctures observed for iron- and copper-modified compounds, different ferroelectric aging mechanisms may be expected based on the one-hand side on the existence of a charged defect dipole and on the other hand on the diffusion of oxygen vacancies to grain boundaries.

3 Donor dopants

In contrast to the *hard*-doping with acceptor-type dopants, for modifications with donor-like dopants (dopants of higher valence than the substituted ion) *soft* compounds with moderate coercive fields result and decreased mechanical quality factor, as well as a higher electromechanical coupling factor. In this case, charge compensation is rather accomplished by the creation of lead vacancies (V''_{Pb}) than by oxygen vacancies.

3.1 Gd^{3+}

One of the most prominent soft-doped compounds is lanthanum-modified PZT ($[Pb_{1-y}La_y][Zr_xTi_{1-x}]O_3$, PLZT $y/x/1-x$), with particular interest for dielectric, piezoelectric and electro-optical applications. As isoelectronic model system for the diamagnetic La^{3+} functional centre, the paramagnetic Gd^{3+} ion may be used. When donor-doping with the trivalent Gd^{3+} ion substituting for the divalent Pb^{2+} ion is considered, the V''_{Pb} created for charge compensation are suspected playing a dominant role in the domain-switching behavior of ceramic oxides, even though no detailed picture is currently available on a microscopic level. Another topic of interest is the discussed ability of *self-compensation* for lanthanide dopants, in which the gadolinium functional centre is incorporated simultaneously on Pb^{2+} and Ti^{4+} sites. Such a self-compensation mechanism has already been suggested for the Gd^{3+} impurity centre in barium titante [78–82] and for PZT 52/48 [83, 84] on the basis of EPR studies. On the other hand, rather a single-site situation has been suggested for a 4 mol % gadolinium-modified PZT powder [85].

The observed single-site EPR spectrum gadolinium-doped $PbTiO_3$ [86] leads to the discussion of conceivable charge compensation mechanisms. As self-compensation or any mechanism involving paramagnetic species can be excluded, the charge compensation mechanism in donor-doped lead titanate can only involve diamagnetic centres, such as V''''_{Ti}, V''_{Pb} or neutral $V^{\times}_{Pb}$. The A^{3+} donor-doping does thus not result in color centers, valency-altered ions, such as Pb^{+} or Ti^{3+} or singly charged lead vacancies V'_{Pb}, all of which are paramagnetic. Concerning the titanium vacancies, which were proposed playing a major role in PLZT compounds of high titanium content [87–89], a coordination close to the gadolinium centre can be excluded as this would reduce the site symmetry to lower than axial; the symmetry being observed experimentally [86]. Consequently, a Schottky-type charge-compensation mechanism has been proposed, that is solely based on the creation of lead vacancies V''_{Pb} and possibly oxygen vacancies as well [86]

$$Gd_2O_3 + TiO_2 \longrightarrow V''_{Pb} + 2Gd^{\bullet}_{Pb} + Ti^{\times}_{Ti} + 5O^{\times}_{O} \qquad (10)$$

Related to the question of charge compensation is the exact site of incorporation of the Gd^{3+} ion in PZT compounds that has been under debate until most recently [85, 90] (S.T. Kirillov, B. Milsch, W. Windsch, unpublished data). By the application of multifrequeny EPR (Fig. 7), a single site $Gd^{\bullet}_{Pb}$ center could be identified [86]. At X-band frequencies (9.4 GHz, Fig. 7(a)), the crystal-field terms are comparable to the electron Zeeman interaction ($B_2^0 \approx \nu_{mw}$) being indicative for a situation in the intermediate-field regime. At Q-band (34 GHz, Fig. 7(b)), EPR is carried out almost in the

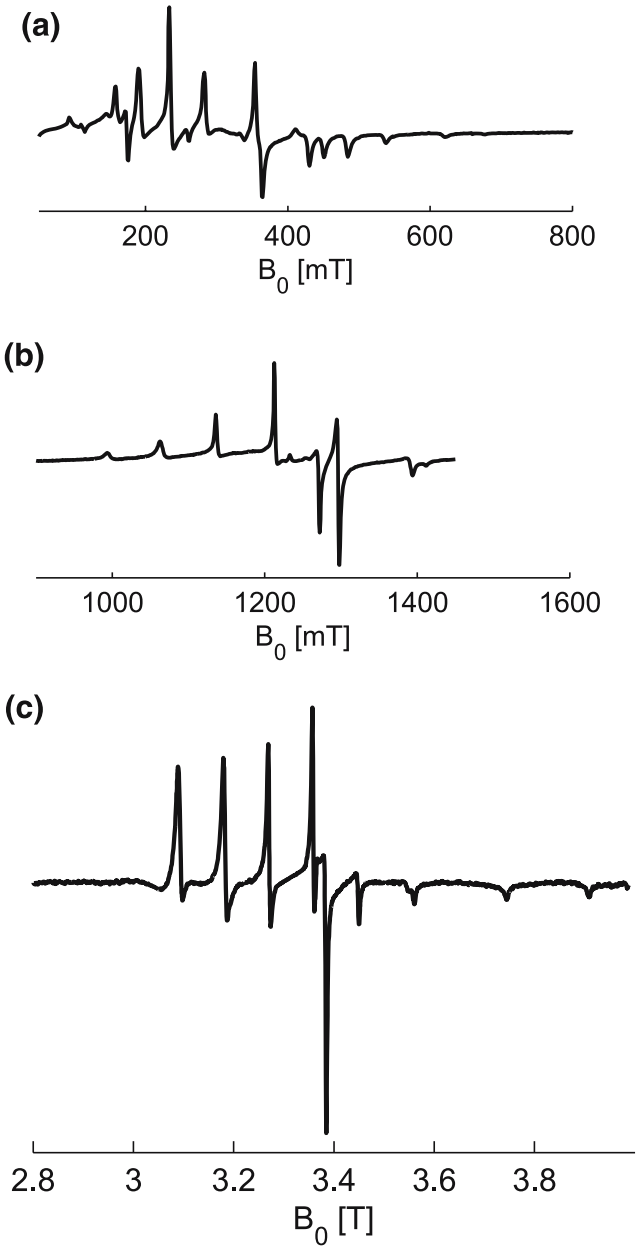

Fig. 7 Multifrequency EPR spectra of the $Gd^{\bullet}_{Pb}$ functional centre in $PbTiO_3$. (**a**) X-band EPR, $\nu_{mw} = 9.4$ GHz. (**b**) Q-band EPR, $\nu_{mw} = 34.42$ GHz. (**c**) W-band EPR ($\nu_{mw} = 94.12$ GHz). Data reproduced from [86]

high-field regime; a situation in which the Zeeman term is the dominant interaction ($B_2^0 \gg \nu_{mw}$). In order to define the sign of the axial fine structure parameter, an experiment has been performed at even higher Larmor frequencies (W-band, 94 GHz, Fig. 7(c)) and at low temperature (5 K) enabling spin polarization in the ground state and determining B_2^0 being positive. By using semi-empirical superposition calculations, it can be deduced from the B_2^0 parameter, that the Gd^{3+} functional center is incorporated on the A-site for $PbTiO_3$, as could have been expected by considering the ionic radii.

As compared to the acceptor-type Fe^{3+} centre in $PbTiO_3$ [23], the observed value for $|B_2^0|$ is more than one order of magnitude smaller, which a priori could have been expected. The reason for this is twofold. Generally, as the 5*s* and 5*d* shells are filled for rare-earth ions, the unpaired 4 *f*-electrons are shielded and form an *inner shell*. They are thus less strongly affected by the surroundings as compared to the 3*d*-electrons in case of transition-metal ions. Moreover, the nearest-neighbor oxygen surrounding is intact in case of Gd^{3+}:$PbTiO_3$, while the iron centre builds a defect associate with an oxygen vacancy, $(Fe'_{Ti} - V_O^{\bullet\bullet})^{\bullet}$ that drastically enhances the local crystal field distortion.

Concerning the question if possible lead vacancies are located in the vicinity of the $Gd^{\bullet}_{Pb}$ center or if they are generated in more distant coordination spheres, high-temperature X-band EPR experiments point to a scenario where the V''_{Pb} are not coordinated to the $Gd^{\bullet}_{Pb}$ functional center. Hence, in donor-doped *soft* lead titanate rather isolated point defects, than charged defect dipoles as in case of *hard* components prevail.

Acknowledgements This research has been financially supported by the DFG centre of excellence 595 *'Electrical Fatigue in Functional Materials'*. Fruitful discussions and helpful support from many colleagues, including Dr. Hans Kungl, Prof. Dr. Michael J. Hoffmann, Prof. Dr. Klaus-Peter Dinse, Dr. Emre Erdem, Prof. Dr. Rolf Böttcher, Dr. Paul Erhard, Prof. Dr. Peter C. Schmidt, Dr. Nina Balke, Prof. Dr. Jürgen Rödel, Dr. Dragan Damjanovic, Dr. Andreas Rüdiger, Dr. Rotraut Merkle, Prof. Dr. Joachim Maier, Dr. Andrew Ozarowski, Dr. Johan van Tol and Dr. Louis Claude Brunel is gratefully acknowledged.

Appendix: EPR spin Hamiltonian

As we deal with different paramagnetic centers, different terms in the spin-Hamiltonian will be relevant. Cu^{2+} has an $3d^9$ electronic configuration, and the spin-Hamiltonian for a single unpaired electron with spin $S = \frac{1}{2}$ can be written as

$$\mathrm{H} = \beta_e \mathbf{B_0} \cdot \mathbf{g} \cdot \mathbf{S} - \beta_n g_n \mathbf{B_0} \cdot \mathbf{I} + \mathbf{S} \cdot \mathbf{A} \cdot \mathbf{I} \qquad (11)$$

in which g_n is the corresponding nuclear g factor and β_e, β_n are the Bohr and nuclear magnetons. The first and second terms represent the electronic and nuclear Zeeman interactions, respectively, where $\mathbf{B_0}$ denotes the external field, given in the principal axes system of the $\mathbf{g}$ matrix. The last term describes the copper hyperfine interaction $\left(I^{^{63,65}\mathrm{Cu}} = \frac{3}{2}\right)$. The nuclear quadrupole interaction does not contribute in first approximation to the EPR spectra and thus has been omitted.

For the high-spin centers Fe^{3+}, $Mn^{2,3,4+}$ and Gd^{3+} with several unpaired electrons in the $3d$ or $4f$ shell, additional fine structure terms in the spin Hamiltonian have to be considered. The crystal field lifts the spin degeneracy resulting in Kramer's doublets and eventually singulets. The degeneracy of the Kramer's doublets may in turn be lifted by an external magnetic field. In this case, an approximate spin-Hamiltonian for high-spin systems can be written as

$$\mathrm{H} = \beta_e \mathbf{B_0} \cdot \mathbf{g} \cdot \mathbf{S} + \sum_{k>2}^{-k\le q\le k} B_k^q \, O_k^q(S_x, S_y, S_z) \qquad (12)$$

Here, the B_k^q are the fine structure Hamiltonian coefficients and O_k^q are the extended Stevens spin operators [71, 91]. The first term again represents the electronic Zeeman interaction and the second term is the effective fine structure Hamiltonian, describing the interaction of the crystal field with the paramagnetic ion. The standard FS parameters B_k^q are related to the also used parameters b_k^q by the scaling factors f_k ($f_2 = \frac{1}{3}$, $f_4 = \frac{1}{60}$) via $B_k^q = f_k b_k^q$ [71]. These values are related to the conventional spectroscopic parameters by $B_2^0 = \frac{b_2^0}{3} = \frac{D}{3}$, $B_2^2 = \frac{b_2^2}{3} = E$, $B_4^4 = \frac{b_4^4}{60} = \frac{5a}{120}$, and $B_4^0 = \frac{b_4^0}{60} = \frac{F}{180} + \frac{a}{120}$ [92, 93]. Corresponding to the site symmetry at which the high-spin ion is incorporated, a subset of all conceivable B_k^q parameters, resulting from 3rd, 4th and 5th-rank tensors, have to be considered [94]. Typically, in the experimental spectra the observed $B_{k>2}^q$ parameters are orders of magnitude smaller than the dominant B_2^q terms. The odd-rank tensor contributions are inherently field-dependent and up to now there has been no experimental evidence for this possible contribution in the class of materials considered.

In case of manganese-doping, an additional hyperfine-coupling term has to be added to the spin Hamiltonian (12) owing to the hyperfine interaction of the electron spins with the nuclear spins of the ^{55}Mn isotope $\left(I^{^{55}\mathrm{Mn}} = \frac{5}{2}\right)$, which is analogous to the third term in Eq. 11.

References

1. B. Jaffe, W.R. Cook, H. Jaffe, *Piezoelectric Ceramics* (Academic, London, 1971)
2. Y. Xu, *Ferroelectric Materials and Their Applications* (Elsevier, Amsterdam, 1991)
3. Y.M. Chiang, D.P. Birnie, W.D. Kingery, *Physical Ceramics—Principles for Ceramic Science and Engineering* (Wiley, New York, 1997)
4. K. Uchino, *Ferroelectric Devices*, (Marcel Dekker, New York, 2000)
5. M.E. Lines, A.M. Glass, *Principles and Applications of Ferroelectrics and Related Materials* (Oxford University Press, Oxford, 2001)
6. A.J. Moulson, J.M. Herbert, *Electroceramics—Materials, Properties, Applications* (Wiley, New York, 2003)
7. S. Sugihara, T. Bak, J. Nowotny, M. Radecka, C.C. Sorrell, J. Mater. Synth. Process. **6**, 335 (1998)
8. H.D. Megaw, *Crystal Structures—A Working Approach*, (Saunders, London, 1973)
9. D.M. Hannon, Phys. Rev. **164**, 366 (1967)
10. R.A. Serway, W. Berlinger, K.A. Müller, R.W. Collins, Phys. Rev. B **16**, 4761 (1977)
11. E. Siegel, K.A. Müller, Phys. Rev. B **19**, 109 (1979)
12. T. Takeda, A. Watanabe, J. Phys. Soc. Jpn. **19**, 1742 (1964)
13. T. Takeda, A. Watanabe, J. Phys. Soc. Jpn. **21**, 1132 (1966)
14. P.V. Lambeck, G.H. Jonker, J. Phys. Chem. Solids **47**, 453 (1986)
15. H. Neumann, G. Arlt, Ferroelectrics **76**, 303 (1987)
16. K. Carl, K.H. H"ardtl, Ferroelectrics **17**, 473 (1978)
17. S. Takahashi, Ferroelectrics **41**, 143 (1982)
18. G. Arlt, H. Neumann, Ferroelectrics **76**, 451 (1987)
19. O.F. Schirmer, W. Berlinger, K.A. Müller, Solid State Commun. **16**, 1289 (1975)
20. R. Waser, T. Bieger, J. Maier, Solid State Commun. **76**, 1077 (1990)
21. C. Ang, Z. Yu, Z. Jing, P. Luckenheimer, A. Loidl, Phys. Rev. B **61**, 3922 (2000)
22. H. Meštrić, R.-A. Eichel, K.-P. Dinse, A. Ozarowski, J. van Tol, L.C. Brunel, J. Appl. Phys. **96**, 7440 (2004)
23. H. Meštrić, R.-A. Eichel, T. Kloss, K.-P. Dinse, So. Laubach, St. Laubach, P.C. Schmidt, Phys. Rev. B **71**, 134109 (2005)
24. R.-A. Eichel, H. Meštrić, K.-P. Dinse, A. Ozarowski, J. van Tol, L.C. Brunel, H. Kungl, M.J. Hoffmann, Magn. Reson. Chem. **43**, S166 (2005)
25. D.J.A. Gainon, Phys. Rev. **134**, A1300 (1964)
26. R.G. Pontin, E.F. Slade, D.J.E. Ingram, J. Phys. C **2**, 1146 (1969)
27. O. Lewis, G. Wessel, Phys. Rev. B **13**, 2742 (1976)
28. V.V. Laguta, M.D. Glinchuk, I.P. Bykov, Y.L. Maksimenko, J. Rosa, L. Jastrabik, Phys. Rev. B **54**, 12353 (1996)
29. G. Arlt, H. Neumann, Ferroelectrics **87**, 109 (1988)
30. S. Pöykkö, D.J. Chadi, Phys. Rev. Lett. **83**, 1231 (1999)
31. R.-A. Eichel, H. Kungl, M.J. Hoffmann, J. Appl. Phys. **95**, 8092 (2004)
32. E. Erdem, R. Böttcher, H.C. Semmelhack, H.J. Gläsel, E. Hartmann, Phys. Status Solidi B **239**, R7 (2003)
33. D.J. Keeble, B. Nielsen, A. Krishnan, K.G. Lynn, S. Madhukar, R. Ramesh, C.F. Young, Appl. Phys. Lett. **73**, 318 (1998)
34. S. Pöykkö, D.J. Chadi, Appl. Phys. Lett. **76**, 499 (2000)
35. E. Cockayne, B.P. Burton, Phys. Rev. B **69**, 144116 (2004)
36. Z. Zhang, P. Wu, L. Lu, C. Shu, Appl. Phys. Lett. **88**, 142902 (2006)
37. P.V. Lambeck, G.H Jonker, Ferroelectrics **22**, 729 (1978)
38. X. Ren, Nat. Mater. **3**, 91 (2004)
39. W.L. Warren, D. Dimos, G.E. Pike, K. Vanheusden, R. Ramesh, Appl. Phys. Lett. **67**, 1689 (1995)
40. W.L. Warren, G.E. Pike, K. Vanheusden, D. Dimos, B.A. Tuttle, J. Robertson, J. Appl. Phys. **79**, 9250 (1996)
41. G. Arlt, P. Sasko, J. Appl. Phys. **51**, 4956 (1980)
42. G. Arlt, D. Hennings, G. de With, J. Appl. Phys. **58**, 1619 (1985)
43. G. Arlt, Ferroelectrics **91**, 3 (1989)
44. T.J. Yan, V. Gopalan, P.J. Swart, U. Mohideen, Phys. Rev. Lett. **82**, 4106 (1999)

45. G.E. Pike, W.L. Warren, D. Dimos, B.A. Tuttle, R. Ramesh, J. Lee, V.G. Keramidas, J.T. Evans, Appl. Phys. Lett. **66**, 484 (1995)
46. D.C. Lupascu, *Fatigue in Ferroelectric Ceramics and Related Issues*, (Springer, Heidelberg, 2004)
47. A.K. Tagantsev, I. Stolichnov, E.L. Colla, N. Setter, J. Appl. Phys. **90**, 1387 (2001)
48. H. Mestric, R.-A. Eichel, K.-P. Dinse, A. Ozarowski, J. van Tol, L.C. Brunel, H. Kungl, M.J. Hoffmann, K.A. Schönau, M. Knapp, H. Fuess, Phys. Rev. B **73**, 184105 (2006)
49. U. Robels, C. Zadon, G. Arlt, Ferroelectrics **133**, 163 (1992)
50. R. Merkle, J. Maier, Phys. Chem. Chem. Phys. **5**, 2297 (2003)
51. R.L. Berney, D.L. Cowan, F. Morin, Solid State Commun. **26**, 579 (1978)
52. R.L. Berney, D.L. Cowan, Phys. Rev. B **23**, 37 (1981)
53. D.J.A. Gainon, J. Appl. Phys. **36**, 2325 (1965)
54. G. Wessel, H. Goldick, J. Appl. Phys. **39**, 4855 (1968)
55. A. Molak, K. Wojcik, Ferroelectrics **125**, 349 (1992)
56. D.J. Keeble, Z. Li, E.H. Poindexter, J. Phys. Condens. Matter **7**, 6327 (1995)
57. H. Ikushima, S. Hayakawa, J. Phys. Soc. Jpn. **27**, 414 (1969)
58. G. Klotzsche, W. Windsch, K. Wojcik, Ferroelectr., Lett. Sect. **15**, 115 (1993)
59. D. Hennings, H. Pomplun, J. Am. Ceram. Soc. **57**, 527 (1974)
60. K. Hayashi, A. Ando, Y. Hamaji, Y. Sakabe, Jpn. J. Appl. Phys. **7**, 5237 (1998)
61. T.Q. Chien, Ph.D. thesis, Universität Leipzig, 1987
62. R. Böttcher, C. Klimm, D. Michel, H.-C. Semmelhack, G. Völkel, H.-J. Gläsel, E. Hartmann, Phys. Rev. B **62**, 2085 (2000)
63. F. Battlo, E. Duverger, J.C. Jules, J.C. Niepce, B. Jannot, M. Maglione, Ferroelectrics **109**, 113 (1990)
64. J. Rödel, G. Tomandl, J. Mater. Sci. **19**, 3515 (1984)
65. D.J. Keeble, Z. Li, M. Harmatz, J. Phys. Chem. Solids **57**, 1513 (1996)
66. O. Bidault, M. Actis, M. Maglione, Solid State Commun. **95**, 845 (1995)
67. W.L. Warren, B.A. Tuttle, F.C. Rong, G.J. Gerardi, E.H. Poindexter, J. Am. Ceram. Soc. **80**, 680 (1997)
68. Z. Bryknar, I.P. Bykov, M.D. Glinchuk, V.V. Laguta, Y.L. Maximenko, Z. Potůček, L. Jastrabik, H.-J. Schulz, Appl. Phys. **A66**, 555 (1998)
69. H.T. Langhammer, T. Müller, R. Böttcher, H.-P. Abicht, Solid State Sci. **5**, 965 (2003)
70. R.-A. Eichel, K.-P. Dinse, H. Kungl, M.J. Hoffmann, A. Ozarowski, J. van Tol, L.C. Brunel, Appl. Phys. A **80**, 51 (2005)
71. A. Abragam, B. Bleaney: *Electron Paramagnetic Resonance of Transition Ions* (Clarendon, Oxford, 1970)
72. M.S. Islam, J. Mater. Chem. **10**, 1027 (2000)
73. S.D. Bernstein, T.Y. Wong, Y. Kisler, R.W. Tustison, J. Mater. Res. **8**, 12 (1992)
74. R. Ramesh, W.K. Chan, B. Wilkens, H. Gilchrist, T. Sands, J.M. Tarascon, V.G. Keramidas, D.K. Fork, J. Lee, A. Safari, Appl. Phys. Lett. **61**, 1537 (1992)
75. Q. Tan, J. Li, D. Viehland, Appl. Phys. Lett. **75**, 418 (1999)
76. T. Friesnegg, S. Aggarwal, R. Ramesh, B. Nielsen, E.H. Poindexter, D.J. Keeble, Appl. Phys. Lett. **77**, 127 (2000)
77. S. Takahashi, Jap. J. Appl. Phys. **20**, 95 (1981)
78. L. Rimai, G.A. de Mars, Phys. Rev. **127**, 702 (1962)
79. T. Takeda, A. Watanabe, J. Phys. Soc. Jpn. **19**, 1742 (1964); *ibid.* **21**, 1132, 1628 (1966)
80. T. Takeda, A. Watanabe, Jpn. J. Appl. Phys. **7**, 3 (1968)
81. T. Takeda, J. Phys. Soc. Jpn. **24**, 533 (1968)
82. T.D. Dunbar, W.L. Warren, B.A. Tuttle, C.A. Randall, Y. Tsur, J. Phys. Chem. B **108**, 908 (2004)
83. S.K.S. Parashar, R.N.P. Choudhary, B.S. Murty, Mat. Sci. Eng. B **110**, 58 (2004)
84. L. Pdungsap, S. Boonyeun, P. Winotai, N. Udomkan, P. Limsuwan, Eur. Phys. J. B **48**, 367 (2005)
85. T.J. Boyle, P.G. Clem, B.A. Tuttle, G.L. Brennecka, J.T. Dawley, M.A. Rodriguez, T.D. Dunbar, W.F. Hammetter, J. Mater. Res. **17**, 871 (2002)
86. R.-A. Eichel, H. Meštrić, H. Kungl, M.J. Hoffmann, Appl. Phys. Lett. **88**, 122506 (2006)
87. D. Hennings, K.H. Härdtl, Phys. Status Solidi A **3**, 465 (1970)
88. K.H. Härdtl, D. Hennings, J. Am. Ceram. Soc. **55**, 230 (1972)
89. R. Holman, Ferroelectrics **10**, 185 (1976)
90. A. Leyderman, V.G. Zaletov, O.E. Fesenko, N.G. Leotiev, V.G. Smotrakov, J. Kor. Phys. Soc. **32**, S703 (1998)
91. C. Rudowicz, Magn. Reson. Rev. **13**, 1 (1987)
92. D.J. Newman, B. Ng, Rep. Prog. Phys. **52**, 699 (1989)
93. C. Rudowicz, S. Madhu, J. Phys. Condens. Matter **11**, 273 (1999)
94. V.G. Grachev, Sov. Phys. JETP **65**, 1029 (1987)